Journal of Physics: Conference Series

PAPER • OPEN ACCESS

Millimeter-wave radar image analysis for the traffic sensing

To cite this article: H M Wu *et al* 2020 *J. Phys.: Conf. Ser.* **1507** 052014

Journal of Physics: Conference Series **1507** (2020) 052014 doi:10.1088/1742-6596/1507/5/052014

Millimeter-wave radar image analysis for the traffic sensing

H M Wu [1] ,F Qi [2,3,4,5], J K Wang [1] and Y Wang [1]

[1] School of communication science and engineering, Northeastern University, Liaoning Province, Shenyang, 110819, China.
[2] Shenyang Institute of Automation, Chinese Academy of Sciences, China
[3] Institutes for Robotics and Intelligent Manufacturing, Chinese Academy of Sciences, China
[4] Key Laboratory of Opto-Electronic Information Processing, Chinese Academy of Sciences, China
[5] Key Lab of Image Understanding and Computer Vision, Liaoning Province, Shenyang, 110016, China

Email:qifeng@sia.cn

Abstract. Millimeter-wave(MMW) radar sensing is one of the most promising technologies to provide safe navigation for autonomous vehicles due to its expected high-resolution imaging capability However, driverless cars have higher request for different environment and light conditions. Therefore, millimetre-wave imaging is of paramount importance for complex load scenario. In this paper, we have built models of pavement pits and bulges and analysed their with differences ways of antennas. A comparison of the imaging performance of experimental systems operating at a MMW radar and a Lidar is presented with the analysis of features for initial image interpretation Experimental images of the complex road surface are made by a 94GHz frequency-modulated continuous-wave (FMCW) radar technique with 3mm wavelength.

1. Introduction

Recently, according to the World Health Organization (WHO), millions of people worldwide die from traffic accidents every year. Among them, nearly 90% of the incidents occurred in low- and middle-income countries. In the future, as vehicles usage increases, this terrible number will increase. Therefore, researching driverless technology is crucial. Driverless vehicle has the potential to improve safety and comfort to road users [1-2]. There are different sensor technologies for driver assistance systems, such as Radars, Lidars, stereo and Infrared cameras to achieve a desired level of performance to support fully autonomous driving [3]. Among them, Lidars and optical cameras are the most widely used; however, they are highly susceptible to obscurants in the air, and changes in the lighting conditions and some extreme weather. Millimeter-wave radars can provide an advantage of robust operation in all weather conditions and in any lighting condition [4-5]. Current automotive radars that operate at 24 and 77 GHz, if used for imaging wouldn’t meet the high resolution compared to optical sensors in driverless. Wide operational bandwidth, this paper studies the 94GHz radar, results in high image resolution [6-7]. Higher frequency radars have smaller antenna sizes, and if achieved, this will result in lower integration costs. The goal of this paper is to demonstrate the imaging performance of experimental millimeter-wave FMCW radar in all terrain scenarios [8].

This paper is organized as follows. In Sections II will briefly introduce the 94GHz radar system structure and FMCW modulation principle. Section III, first, simulation and experimental analysis of road pits. Then, based on the analysis of the characteristics of complex road conditions, a method of initial image interpretation is proposed. Three-dimensional imaging capabilities are further discussed in Section IV, here, the potential to rehabilitate high resolution 3D imaging by vehicles. The MMW radar and Lidar are used to compare the three-dimensional imaging of the building. In Section V conclusions are drawn, and further system development is discussed.

2. Radar System

2.1. Radar structure

The basic architecture of the 94GHz FMCW radar is shown in figure 1, which simplified block diagram. The LFM base band. signal with a C band wave source. First, the wave source enters the power amplifier, followed by a 13 multiplier, an isolator, a bandpass filter, a mixer, and finally waves are transmitted through the antenna. The millimeter wave radar has a special unbalanced pass-through mixer. It is configured so that about 2% of the LO power passes through the mixer to the RF port, and it is used as transmit power for the radar. A band analog-to-digital converter (ADC) is used for sampling and passes the data to Digital Signal Processor(DSP).

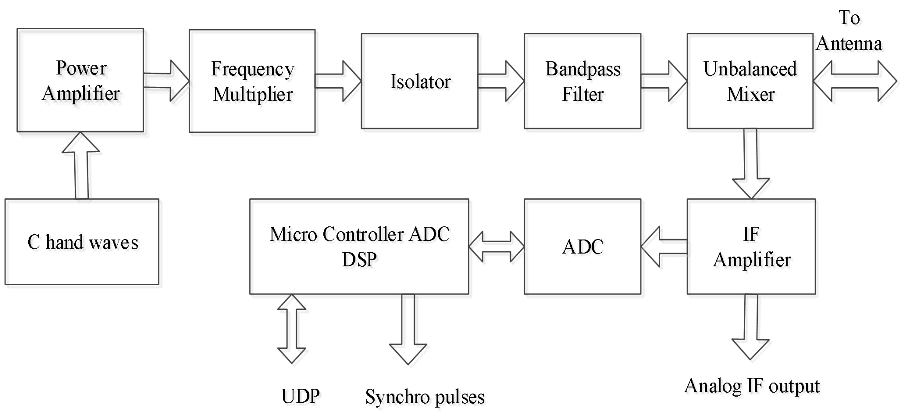

Figure 1. Block diagram of 94 GHz radar.

Table 1 shows the main parameters of the radar system. a comparison of the imaging performance of experimental systems operating at cassegrain antenna and horn antenna.

Table 1. System parameter.

Parameter	Value
Detection Range	0.15 to 150 m
Transmitter emission power	2-5 mW
Noise figure of receiver	13 dB (max)
Cassegrain antenna gain	42dBi
Cassegrain antenna beam width	1 deg
Horn antenna gain	25dBi
Horn antenna beam width	7 deg

2.2. FMCW Radar and the Range Resolution
When the transmitted pulse is a narrow pulse, the radar can distinguish the target distance very well. In other words, the pulse width of the target echo signal affects the radar's range resolution. To solve this contradiction, FMCW modulation is one of the most commonly used methods. In FMCW radar, the transmitted signal is a chirped continuous wave, as shown in equation (1):

$$S_{Tx}\left(t\right)=A\cos\left(2\pi f_0 t+\pi k t^2\right) \tag{1}$$

A represents the amplitude value of the transmitted signal, f0 is the starting frequency, and is the frequency modulation slope. After being by the transmitting antenna, the object reflects the echo signal after encountering the object. The back scattered signal is a chirped continuous wave, as shown in equation (2):

$$S_{Rx}\left(t\right)=\cos(2\pi f_0\left(t-t_0\right)+\pi k(t-t_0)^2) \tag{2}$$

After mixing, the signal passes through a low-pass filter to find the beat signal, and its expression is given by equation (3):

$$S_{Beat}=\cos\left(2\pi f_0 t_0+2\pi k t_0 t-\pi k t_0^2\right) \tag{3}$$

After the FFT of the time domain's beat signal, The peak value of this signal can be used to find the corresponding distance. The distance is given by equation (4):

$$\triangle R=\frac{c}{2}\triangle\tau=\frac{c}{2k}\triangle f_{\mathrm{Beat}}=\frac{Tc}{2BW}\triangle f_{Beat}=\frac{\mathrm{c}}{2\mathrm{B}} \tag{4}$$

3. Imaging of Road Scenarios by 94GHz Radar

3.1. Road pit simulation and experiment
As shown in figure 2, it is the electric field simulation diagram of the road pit. The antenna transmission frequency is 94GHz and is 1.2m away from pit. The antenna has a depression angle of 14 degrees, and the transmitted signal is exactly the same as the position of the road pit. Asphalt is selected as the pavement material because it is the most commonly used one, and the dielectric constant of it is 2.6. Two lines (A and B) are taken from the pit and observed the electric field changes, as shown in figure 3a-3b. figure 3a is the electric field diagram of the upper surface of the pit. It can be seen from the figure that the electric field strength on both sides is strong, and the middle is weak, with a maximum value of about 67(V/m). The cause of this phenomenon is that most of the electric field strength transmits into the pit. figure 3b, as the electric field diagram of the inside, indicates that the strength is increasing, and the maximum value is around 73(V/m). This is because after several times of diffraction, the electric field strength is stronger than the previous. It proves that the pit can be identified by radar.

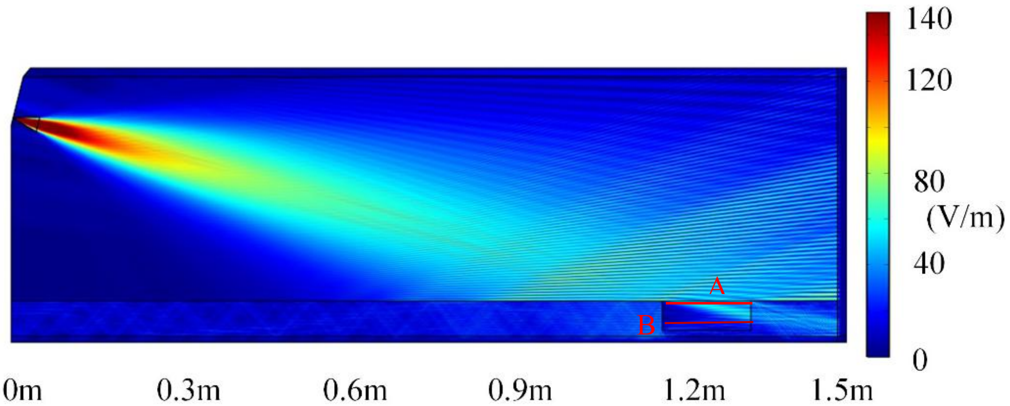

Figure 2. Electric field simulation diagram of the road pit.

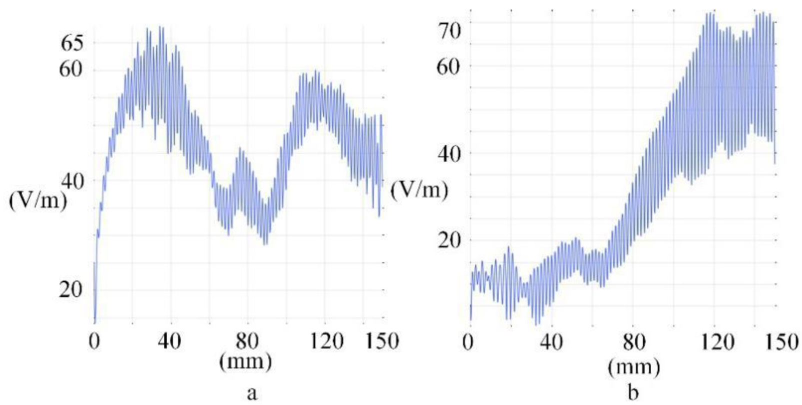

Figure 3. Electric field diagram of the upper surface and inside of the pit.

Figure 4 is the original picture of the pit. The distance between the pit and the radar is 10m. The pit is 25cm in diameter and 10cm in depth, and on each side of the pit there are two manholes, which are referential objects. The road is scanned from -15° to $+15^\circ$ clockwise with 0.1° steps. In this experiment, a horn antenna (as shown in figure 5a), a cassegrain antenna (as shown in figure 5b), and an absorbing material to block the top and bottom of a cassegrain antenna (as shown in figure 5c) are used to compare the two-dimensional imaging of the road pit. The advantage of blocking the third one, which can be seen as an H-plane horn, is to achieve narrower beam width at the azimuth distance. As shown in figure 5a, the pit cannot be identified because the horn antenna beam width, which is 7 degree, is broad. However, in figure 5b and figure 5c, the pit is able to be identified. In addition, the resolution of figure 5c is higher because vertically its light spot is oval and more information from the target backscatter can be gained.

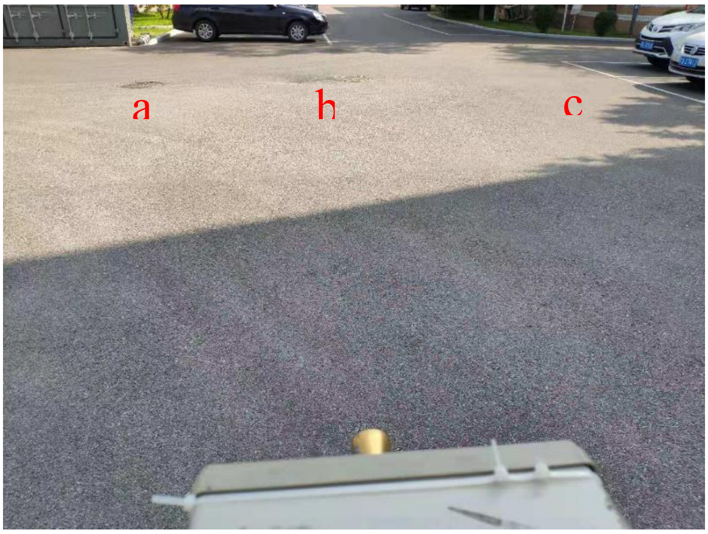

Figure 4. the original picture of pit.

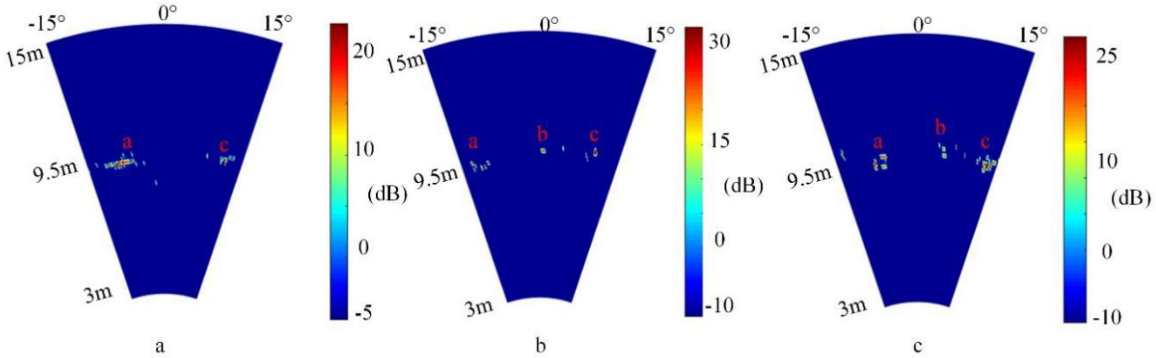

Figure 5. the imaging diagram of pit.

3.2. Complex road conditions experiment

As shown in figure 6, it is a complex road with sand, a brick, a metal ball, and a roadblock. The sand is 1m in length, 0.5m in width, and 11m away from the radar. The brick is 20cm in length, 10cm in width, and 14m away. 17m away there is the metal ball, which is 30cm in diameter. At a distance of 20m, there is a roadblock, which is 60cm in height. The scenario is scanned from −15◦ to +15◦ clockwise with 0.1◦ steps. The experiment also adopts the above-mentioned three ways of imaging, as demonstrated in figure 7a-7c. The imaging of horn antenna cannot be discerned the brick, roadblock and kerb, in figure 7a. Returns from the tow kerbs are seen as nearly continuous linear features on the image approaching optical quality, as shown in figure 7b and figure 7c. However, under the same scanning angle, the range of imaging without blocking the antenna is wider than blocking the antenna. It is worth noting that the increased diffused scattering of a MMW radar signal allows distinguishing smoother patches on the generally rough surface of the road.

Figure 6. the original picture of complex road.

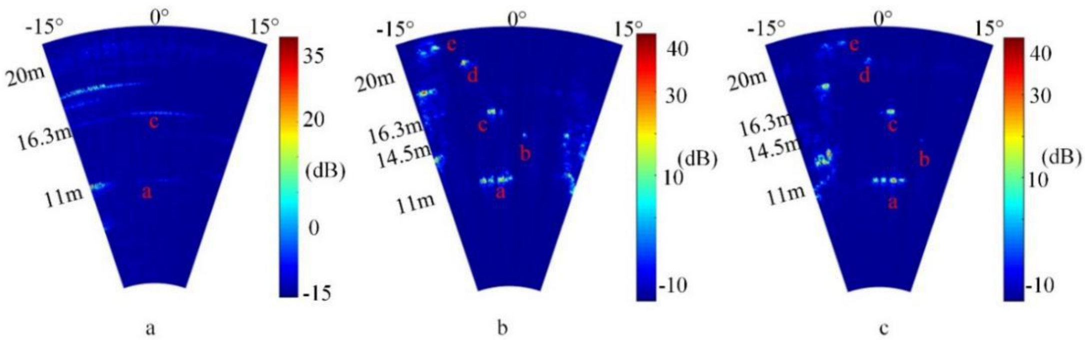

Figure 7. the imaging diagram of complex road.

4. 3D Imaging by 94GHz Radar

4.1. Imaging of different vehicle styles

94GHz radar is used for imaging a 11m distance A-type vehicle and a 12m distance A0-type vehicle. Imaging results are shown in figure 8a-8d. The scenario is scanned from −15◦ to +15◦ clockwise at the horizontal direction, azimuth angle of 16 degrees, with 0.1◦ steps. From the imaging results, the length error of the A type vehicle is 1.55% , and the length error of the A0 type vehicle is 3.1% .These results are consistent with the actual length value. It can be clearly seen that the A0-type vehicle has no trunk, which is the same as the actual situation. However, the trunk is clearly visible in Figure 8c. Therefore, the radar can clearly distinguish the A and A0 models vehicle.

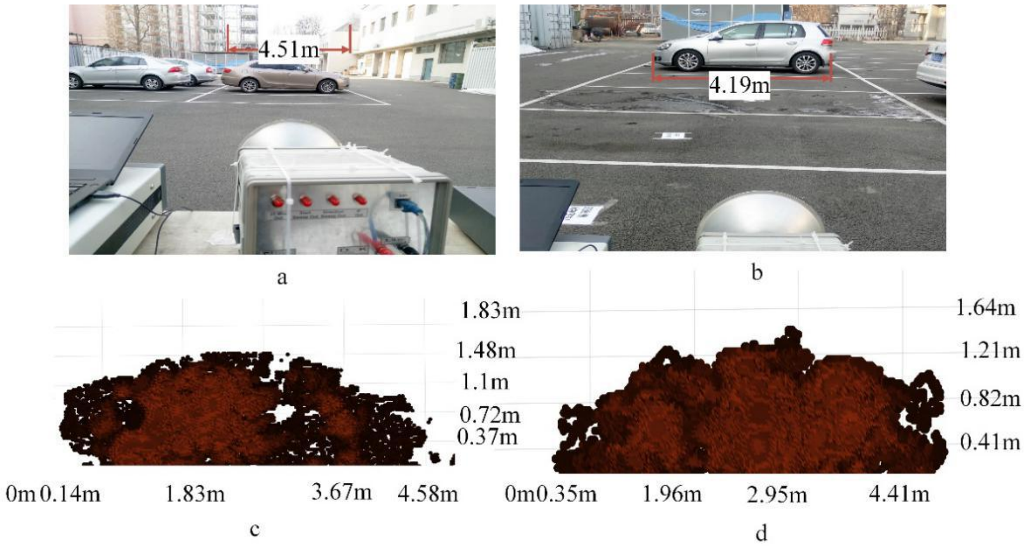

Figure 8. 3D imaging of vehicles.

Finally, the radar performs three-dimensional imaging at a 140m distance building. The imaging results are shown in figure9. The scanning range is horizontal angle of 16 degrees, azimuth angle of 20 degrees, and step length is 0.1 degrees. From imaging results The semi-circular building can be clearly distinguished.

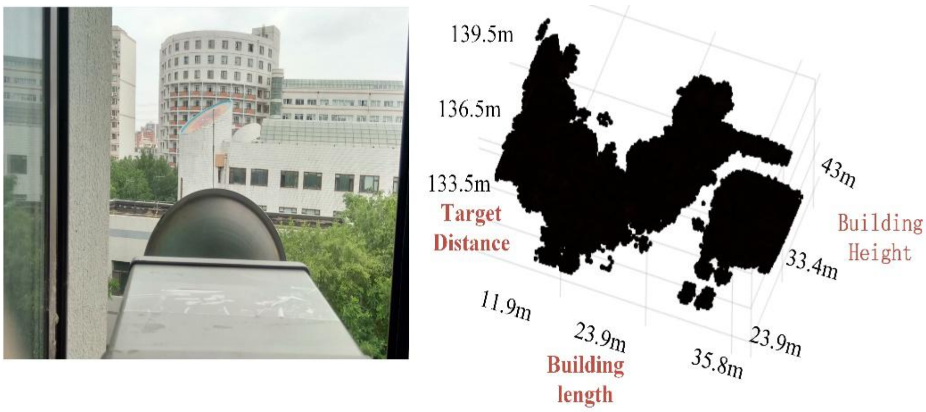

Figure 9. 3D imaging of the building.

4.2. *Comparison imaging of the MMW radar and Lidar*

MMW radar and lidar are used for imaging a 44m distance structure. The scenario is scanned from −40◦ to +40◦ clockwise at the horizontal direction, azimuth angle of 25 degrees, with 0.2◦ steps. figure 10 is the original picture of the structure. The building is surrounded by glass. As shown in figure 11a-11b, it is 3D imaging map of MMW radar and Lidar. From the imaging results, MMW radar is much better than Lidar. The cause of this phenomenon is that Lidar's performance suffers in the strong lighting conditions. Lidar mainly detects the position of a target by emitting some laser beam. The laser beam is weakened in the glare environment.

Figure 10. the original picture of the structure.

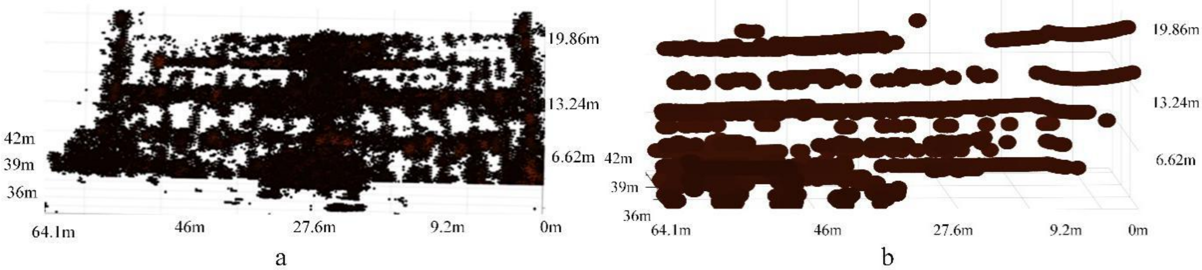

Figure 11. 3D imaging map of MMW radar and Lidar.

5. Conclusion

The initial 94-GHz experimental results demonstrate the potential of a MMW radar sensor to deliver a high-resolution image of the road environment due to it sensitivity even to slight roughness and texture of the imaged objects. It has been shown that different imaging of complex road is compared with three ways of antennas, and contrasted MMW radar with Lidar. The experimental results fully highlight the advantages of MMW radar in driverless. Enhanced automatic feature detection will be possible by using further image processing and feature extraction techniques. In the next stage of this research, the performance of extreme weather will be analyzed for outdoor 3D imaging by MMW radar and Lidar.

References

[1] K B Cooper, R J Dengler and N Llombart 2008 *IEEE Trans. Microwave Theory and Tech Penetrating* **56** 2771-8

[2] A Mostajeran, A Cathelin and E Afshari 2017 *IEEE J. Solid-State Circuits* **10** 2721–34
[3] B B Cheng et al.2013 *IEEE Trans. THz Sci. Technol* **5** 594–605
[4] D Jasteh, E G Hoare, M Cherniakov and M Gashinova 2016 *IEEE Geosci. Remote Sens. Lett.* **4** 490–4
[5] Fatemeh Norouzian , Rui Du and Edward G 2018 *IEEE Transactions on Teraherta Science and Technology* **1** 63-75
[6] M Moallem and K Sarabandi 2014 *IEEE Trans. Antennas Propag* **1** 500–4
[7] K Y Guo, E G Hoare and D Jasteh 2015 *IEEE Trans. Intell. Transp. Syst* **2** 825–33
[8] D R Vizard et al., 2014 *IEEE CAMA, Antibes Juan-les-Pins* 1–4